

Plasma-Based Generation and Control of a Single Few-Cycle High-Energy Ultrahigh-Intensity Laser Pulse

M. Tamburini,^{1,*} A. Di Piazza,¹ T. V. Liseykina,² and C. H. Keitel¹

¹*Max-Planck-Institut für Kernphysik, Saupfercheckweg 1, D-69117 Heidelberg, Germany*

²*Institut für Physik, Universität Rostock, D-18051 Rostock, Germany*

(Dated: August 24, 2018)

A laser-boosted relativistic solid-density paraboloidal foil is known to efficiently reflect and focus a counterpropagating laser pulse. Here we show that in the case of an ultrarelativistic counterpropagating pulse, a high-energy and ultrahigh intensity reflected pulse can be more effectively generated by a relatively slow and heavy foil than by a fast and light one. This counterintuitive result is explained with the larger reflectivity of a heavy foil, which compensates for its lower relativistic Doppler factor. Moreover, since the counterpropagating pulse is ultrarelativistic, the foil is abruptly dispersed and only the first few cycles of the counterpropagating pulse are reflected. Our multi-dimensional particle-in-cell simulations show that even few-cycle counterpropagating laser pulses can be further shortened (both temporally and in the number of laser cycles) with pulse amplification. A single few-cycle, multi-petawatt laser pulse with several joule of energy and with peak intensity exceeding 10^{23} W/cm² can be generated already employing next-generation high-power laser systems. In addition, the carrier-envelope phase of the generated few-cycle pulse can be tuned provided that the carrier-envelope phase of the initial counterpropagating pulse is controlled.

PACS numbers: 52.59.Ye, 52.38.-r, 52.65.Rr, 42.65.Re

A wide range of novel studies in nonlinear optics as well as the major new regimes of extreme field physics require laser pulses which simultaneously exhibit the following three key features: few-cycle duration, high-energy and ultrahigh intensity. Already in nonrelativistic atomic physics, it has been demonstrated that quantum processes can be controlled by manipulating the pulse shape of few-cycle laser pulses [1]. In order to achieve the same goal also in the ultrarelativistic regime and in the realm of nonlinear QED, few-cycle laser pulses with tunable carrier-envelope phase (CEP) are required with peak intensities largely exceeding 10^{20} W/cm² [2–4]. At such high intensities, for example, the nonlinear Compton emission spectrum is expected to show pronounced pulse-shape effects [5, 6].

Although next-generation 10-PW optical laser systems are expected to generate laser pulses with 150-300 J energy and 15-30 fs duration [4, 7] [full-width-at-half-maximum (FWHM) of the pulse intensity], the limited bandwidth renders the generation of few-cycle pulses with multi-joule energy very challenging [8, 9]. Indeed, the only laser system aiming at 1-PW power and few-cycle duration is the Petawatt Field Synthesizer [10]. Several methods for further shortening and amplifying laser pulses have been proposed, e.g., Raman [11, 12] and Brillouin [13, 14] backscattering, interaction with plasma waves [15, 16] and ionization induced self-compression effects [17, 18]. However, none of the pulses generated employing the above-mentioned methods simultaneously exhibit few-cycle duration, multi-joule energy and ultrarelativistic intensity. In fact, the initial intensity is bounded to relatively moderate values and the generated pulses are transversely and temporally modulated, which might

prevent their subsequent focusing to ultrarelativistic intensities. In addition, the CEP control, which is crucial for many applications, has not been demonstrated in any of the above-mentioned methods.

In this Letter, we put forward the concept of a laser-boosted solid-density paraboloidal relativistic “mirror”, interacting with a superintense counterpropagating laser pulse, to generate a CEP tunable few-cycle pulse with multi-joule energy and peak intensity exceeding 10^{23} W/cm². Contrary to intuition, it is found that a heavy and therefore relatively slow “mirror” should be employed to maximize the intensity and the energy of the reflected pulse, since its larger reflectivity compensates for the lower velocity. Furthermore, the short duration of the reflected pulse is achieved by employing a superintense incident pulse, which abruptly disperses the plasma mirror after only the first few cycles. Multi-dimensional particle-in-cell (PIC) simulations indicate both the feasibility of the presented setup by employing next-generation multi-PW laser systems and a considerable shortening with amplification even for already few-cycle laser pulses.

In the proposed setup, a “driver” pulse with frequency ω and (average) intensity I_d accelerates a “mirror” to relativistic velocities along the positive x direction and a “reflected” pulse is generated in the collision of the mirror with a counterpropagating “source” pulse, also with frequency ω and with intensity I_s . Here and below, the subscript s (d) and the upper (lower) sign refer to the source (driver) pulse counterpropagating (copropagating) with respect to the mirror, and $T = 2\pi/\omega$ ($\lambda = cT$) is the laser period (wavelength). Our aim here is to determine the conditions for maximizing both the intensity and the en-

ergy of the reflected pulse. In order to develop an analytical model, for the thin foil we employ the Dirac- δ density profile $n(x) = n_e \ell \delta(x)$ [19, 20], where n_e and ℓ are the foil density and thickness, respectively. If the foil moves with velocity $v_x = \beta c > 0$, its reflectivity is given by $\mathcal{R}_{s/d} = \zeta_{s/d}^2 / (\zeta_{s/d}^2 + \Gamma_{s/d}^2)$ [20], where $\Gamma_{s/d}^2 = \{1 + a_{s/d}^2 - \zeta_{s/d}^2 + [(1 + a_{s/d}^2 - \zeta_{s/d}^2)^2 + 4\zeta_{s/d}^2]^{1/2}\} / 2$ and $\zeta_{s/d} \equiv \zeta_0 / D^\pm$. Here we have introduced the normalized (average) field amplitude $a_{s/d}^2 \equiv I_{s/d} / I^*$ with $I^* \equiv m_e^2 \omega^2 c^3 / 4\pi e^2$, the Doppler factors $D^\pm = \sqrt{(1 \pm \beta) / (1 \mp \beta)} \gtrless 1$, and the surface density $\zeta_0 \equiv \pi n_e \ell / n_c \lambda$, with $n_c \equiv m_e \omega^2 / 4\pi e^2$ being the critical density. Notice that for a linearly polarized (LP) pulse the peak intensity \hat{I} is approximately twice the intensity I , whereas they coincide for a circularly polarized (CP) pulse. If both the source and the driver pulse fields are ultrarelativistic ($a_{s/d} \gg 1$), the reflectivity can be approximated as [20, 21]: $\mathcal{R}_{s/d} \approx 1$ if $\zeta_{s/d} > a_{s/d}$ and $\mathcal{R}_{s/d} \approx \zeta_{s/d}^2 / a_{s/d}^2$ if $\zeta_{s/d} < a_{s/d}$, which presents the reflectivity with accuracy better than 2% for $a_{s/d} > 50$. Hence, the condition $\zeta_{s/d} > a_{s/d}$ has to be fulfilled to secure $\mathcal{R}_{s/d} \approx 1$.

In our model the foil is initially at rest and it is accelerated along the positive x direction by the driver pulse. In order to determine the value of the Doppler factor after the acceleration phase D_0^+ , we assume that $\zeta_0 > a_d$ and thus $\mathcal{R}_d \approx 1$. The velocity of a foil accelerated by the radiation pressure [22] of the driver pulse can be calculated analytically by employing the ‘‘light sail’’ equation for a perfectly reflecting mirror [20, 21, 23] and the result for D_0^+ is $D_0^+ = 1 + \mathcal{E}_d / \zeta_0$, where $\mathcal{E}_d = 2\pi Z m_e \int a_d^2(w) dw / Am_p$ is the ‘effective’ energy of the driver pulse. Here Z (A) is the ion atomic number (weight) and $a_d^2(w) = I_d(w) / I^*$ is the field amplitude as a function of the foil phase $w = [t/T - x(t)/\lambda]$.

Since the foil undergoes a recoil due to the radiation pressure of the source pulse, the Doppler factor D^+ of the foil at the maximum of the source pulse intensity is smaller than D_0^+ . On this respect it is convenient to employ a sharp-rising, high-contrast source pulse, as those generated with the plasma mirror technique [24, 25]. By proceeding as for the calculation of D_0^+ , we obtain

$$D^+ = \frac{D_0^+}{1 + D_0^+ \mathcal{E}_s / \zeta_0} = \frac{\zeta_0 (\zeta_0 + \mathcal{E}_d)}{\zeta_0^2 + \mathcal{E}_s (\zeta_0 + \mathcal{E}_d)}, \quad (1)$$

where $\mathcal{E}_s = 2\pi Z m_e \int a_s^2(w) dw / Am_p$ which, for a sharp-rising pulse, is the part of the source pulse energy before the source pulse intensity reaches its maximum (see page 4 for details). Since we seek $\mathcal{R}_s \approx 1$, we require $\zeta_s > a_s$, which provides the constraint $\zeta_0 > \zeta_{0,m}$ with

$$\zeta_{0,m} = a_s [1 - \epsilon + \sqrt{(1 - \epsilon)(1 - \epsilon + 4\mathcal{E}_d / a_s)}] / 2, \quad (2)$$

where $\epsilon \equiv \mathcal{E}_s / a_s$ accounts for the effect of the recoil. In order to maximize the energy and the intensity of the reflected pulse at $\mathcal{R}_s \approx 1$ for fixed driver and source pulses,

we have to maximize the Doppler factor D^+ as a function of ζ_0 with the condition $\zeta_0 > \zeta_{0,m}$. From Eq. (1), $D^+(\zeta_0)$ has a maximum at $\zeta_0^* = \mathcal{E}_d \sqrt{\mathcal{E}_s} / (\sqrt{\mathcal{E}_d} - \sqrt{\mathcal{E}_s})$ and monotonically decreases for $\zeta_0 > \zeta_0^*$. Assuming sufficiently small recoil [$\epsilon < 1/2$ and $\mathcal{E}_d > \mathcal{E}_s(1 - \epsilon)^2 / (1 - 2\epsilon)^2$], then $\zeta_{0,m} > \zeta_0^*$ and the maximum $D^+(\zeta_0)$ compatible with $\zeta_0 > \zeta_{0,m}$ is at $\zeta_{0,m}$, and it is $D_m^+ = \zeta_{0,m} / a_s$.

Note that, for a flat foil and fixed driver and source pulses, both the maximum intensity $I_r = D^{+4} \mathcal{R}_s I_s$ and energy $E_r \approx I_r S \Delta t_s / D^{+2}$ of the reflected pulse are achieved at the minimum ζ_0 such that $\zeta_s > a_s$, i.e. at $\zeta_{0,m}$. Here S is the surface area of the focal spot and Δt_s is the source pulse duration. In fact, for $\zeta_s < a_s$ the reflectivity is $\mathcal{R}_s \approx \zeta_s^2 / a_s^2$ thus $I_r = D^{+2} \zeta_0^2 I^*$ and $E_r \approx \zeta_0^2 I^* S \Delta t_s$, which are monotonically increasing functions of ζ_0 . The fact that there exists an optimal value of the surface density has a simple physical interpretation: for fixed driver and source pulses, if ζ_0 is too large, the foil slows down and the Doppler factor is small. If ζ_0 becomes too small, the velocity of the foil increases and the reflectivity rapidly decreases because ζ_s tends to vanish. Moreover, at $\zeta_{0,m}$ the reflected pulse energy $D_m^{+2} I_s S \Delta t_s$ is a monotonically increasing function of I_s . If $\epsilon < 1/3$ and $\mathcal{E}_d < a_s(1 - \epsilon)^2(1 - 3\epsilon) / 4\epsilon^2$, i.e. if the effect of the recoil is sufficiently small, the maximum reflected pulse intensity $D_m^{+4} I_s$ is also a monotonically increasing function of I_s . For fixed source pulse, the above conditions account for the slowdown of the foil due to the recoil, which becomes increasingly important for increasing foil velocity [see Eq. (1)]. In a three-dimensional (3D) geometry, a paraboloidal mirror can focus the source pulse to its diffraction limit. Since the laser wavelength is Doppler reduced in the rest frame of the foil, the reflected pulse can be focused down to λ^2 / D^{+2} and the intensity at the focus is $I_{r,f} = D^{+6} \mathcal{R}_s I_s S / \lambda^2$. If $\zeta_0 > \mathcal{E}_d$, $\epsilon < 1/4$ and $\mathcal{E}_d < 2a_s(1 - \epsilon)^2(1 - 4\epsilon) / (1 + 2\epsilon)^2$, the maximum of the intensity at the focus $I_{r,f}$ is achieved at $\zeta_{0,m}$ and it is an increasing function I_s . In other cases, the maximum of $I_{r,f}$ can be a decreasing function of I_s or the maximum of $I_{r,f}$ can be achieved at $\mathcal{R}_s < 1$. However, in these cases a higher intensity *at the focus* is achieved at the expense of a lower reflected pulse power $P_r = D^{+4} \mathcal{R}_s I_s S$ and energy $E_r \approx D^{+2} \mathcal{R}_s I_s S \Delta t_s$.

For simplicity, we first consider a driver and source pulse with one-cycle \sin^2 -function rise and fall, and with a five-cycle constant plateau. Figure 1 reports the maximum reflected pulse amplitude $\sqrt{D^{+4} \mathcal{R}_s I_s} / I^*$ as a function of ζ_0 for $a_d = 130$ and for $a_s = 130, 100, 80$. In each case the reflected pulse amplitude initially increases for increasing ζ_0 , reaches its maximum at $\mathcal{R}_s \approx 1$, and then decreases as the Doppler factor decreases. The three triangles in Fig. 1 are centered at $(\zeta_{0,m}, \sqrt{D_m^{+4} I_s} / I^*)$ and their position coincides with the maximum of the reflected pulse amplitude, confirming our analytical estimates. Since in all cases $\mathcal{E}_d < a_s(1 - \epsilon)^2(1 - 3\epsilon) / 4\epsilon^2$, the

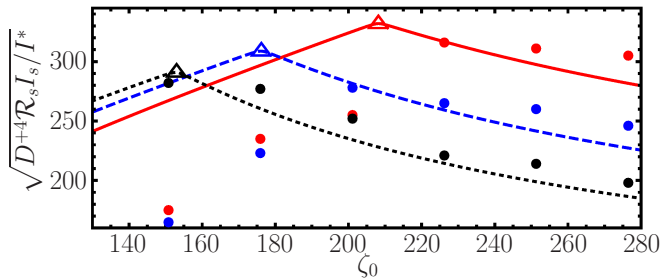


FIG. 1. (color online). The maximum amplitude of the reflected pulse $\sqrt{D^{+4}\mathcal{R}_s I_s/I^*}$ as a function of ζ_0 for $a_d = 130$ and $a_s = 130$ (solid red line), $a_s = 100$ (dashed blue line) and $a_s = 80$ (dotted black line). See the text for further details.

maximum reflected amplitude rises for increasing I_s (see Fig. 1). The results of one-dimensional (1D) PIC simulations with CP driver and the source pulses are also reported in Fig. 1 (colored circles), the foil being a slab of fully ionized carbon with $n_e = 400n_c$. The spatial resolution is $\lambda/4000$ and the number of particles per cell per species 1000. Our PIC simulation results agree with the model predictions at $\zeta_0 > \zeta_{0,m}$, i.e. at $\mathcal{R}_s \approx 1$.

In a multidimensional geometry, the onset of transverse Rayleigh-Taylor-like (RT) [22] instabilities renders the foil ‘porous’ to the source pulse. RT instabilities in the radiation pressure acceleration regime have been investigated analytically [26, 27], numerically [26–28] and experimentally [29]. In particular, in Refs. [26, 27] it was shown that in the linear approximation the RT instability grows as $\exp[\Phi_d(w)]$ with $\Phi_d(w) = \int_0^w 2\pi[Zm_e a_d^2(u)\lambda/Am_p \zeta_0 \lambda_{RT}]^{1/2} du$ where λ_{RT} is the wavelength of the perturbation. Our simulations indicate that in order to effectively reflect the source pulse, $\Phi_d(w) \lesssim 5.7$ for $\lambda_{RT} \approx \lambda$ [29], which can be fulfilled by increasing the value of $\zeta_0 > \zeta_{0,m}$.

In our two-dimensional (2D) PIC simulations both the driver and the source pulse have a \sin^2 -function temporal field profile with 15.5 fs duration (FWHM of the intensity), Gaussian transverse profile and wavelength $\lambda = 800$ nm. The driver (source) pulse is CP (LP with the electric field along the y axis) with intensity $I_d \approx 3.4 \times 10^{22}$ W/cm² ($I_s \approx 5.6 \times 10^{22}$ W/cm²) and spot radius $\sigma_d = 3.8\lambda$ ($\sigma_s = 1.2\lambda$), corresponding to a power $P_d \approx 9.9$ PW ($P_s \approx 1.6$ PW). These parameters are envisaged at the APOLLON laser system [4, 7, 30]. The foil consists of fully ionized carbon with electron density $n_e = 400n_c$ and it is initially shaped transversely with a thickness distribution $\ell = \max[\ell_1, \ell_0 \exp(-y^2/2\sigma_f^2)]$, with $\ell_1 = 0.02\lambda$, $\ell_0 = 0.20\lambda$, $\sigma_f = 2.6\lambda$ and localized at $x = 5\lambda$. Note that the properties of such carbon foils can be engineered with high precision nowadays [31, 32]. It has been shown that Gaussian pulses and shaped foils can be employed to generate collimated ion beams [33, 34]. Here we propose to use shaped foils

to generate paraboloidal relativistic mirrors. Indeed, for $\sigma_d > \sqrt{2}\sigma_f$ the acceleration factor $a_d^2(y)/\zeta_0(y)$ [33] is larger in the outer part of the foil, which therefore takes a focusing profile for the source pulse. Since for many applications slow focusing and defocusing are desirable, we have set $\sigma_d \approx \sqrt{2}\sigma_f$ so the relativistic mirror is nearly flat before interacting with the source pulse (see Fig. 2). The size of the computational box is $20\lambda(x) \times 20\lambda(y)$, the corresponding grid is $20000(x) \times 8000(y)$ and 900 particles per cell for each species are used.

Figure 2 displays the evolution of the square root of the energy density $u = \sqrt{(\mathbf{E}^2 + \mathbf{B}^2)}/2$ and of the electron density distribution n_e . The driver (source) pulse reaches the edge of the foil at $t \approx 0$ ($10T$). An accurate synchronization between two laser pulses can be achieved, e.g., by generating the two pulses from the same seed pulse before the amplification stage. Although instabilities have developed ($\Phi_d \approx 4.7$ with our parameters) and density fluctuations are clearly visible before the source pulse impinges on the foil, the foil remains sufficiently compact to reflect the first part of the source pulse (see Fig. 2 at $t \leq 16T$ and the Supplemental Material [URL] for a movie of the laser-foil interaction). As the source pulse amplitude at the foil position increases, the source pulse ‘digs through’ the lower-density regions and abruptly disperses the foil, which becomes transparent to the remaining part of the pulse (see Fig. 2 from $t = 16T$ to $t = 18T$). Finally, at $t = 22T$ a single few-cycle reflected pulse separated from the foil remnants is observed. The peak intensity and peak power of the reflected pulse are: $\hat{I}_r \approx 2.3 \times 10^{23}$ W/cm² (for the source pulse $\hat{I}_s \approx 9.6 \times 10^{22}$ W/cm²), and $\hat{P}_r \approx 2.2$ PW, with 5.8 fs duration and 6.8 J energy [see Fig. 3(c)]. Figure 3(a) displays the y component of the electric field of the reflected pulse along the central axis for the case of zero (solid, black line) and $\pi/2$ (dotted, red line) CEP of the source pulse showing that the reflected pulse inherits the CEP of the source pulse. Inclusion of radiation reaction (RR) effects, according to Refs. [35, 36], does not significantly alter the reflected pulse [see Fig. 3(b)]. Our explanation is that when the reflected pulse is generated, the foil density is still high and the fields inside the foil are much smaller than in vacuum [35]. Moreover, we ensured that the probability of electron-positron pair production remains negligible. The influence of a randomly distributed preplasma on the front surface of the foil is also considered in Fig. 3(b) (dashed, red line). The preplasma thickness corresponds to 10% of the foil thickness and its average density is $n_e/2$. The presence of the preplasma reduces the peak intensity, peak power and energy of the reflected pulse to $\hat{I}_r \approx 1.8 \times 10^{23}$ W/cm², $\hat{P}_r \approx 2.0$ PW and 5.8 J, respectively. This can be explained by the increased electron heating due to the enhanced penetration of the driver pulse into the preplasma. The modulus of the Fourier transform of the y component of the electric field along the central axis $|E_{r,y}(k_x)|$, where k_x

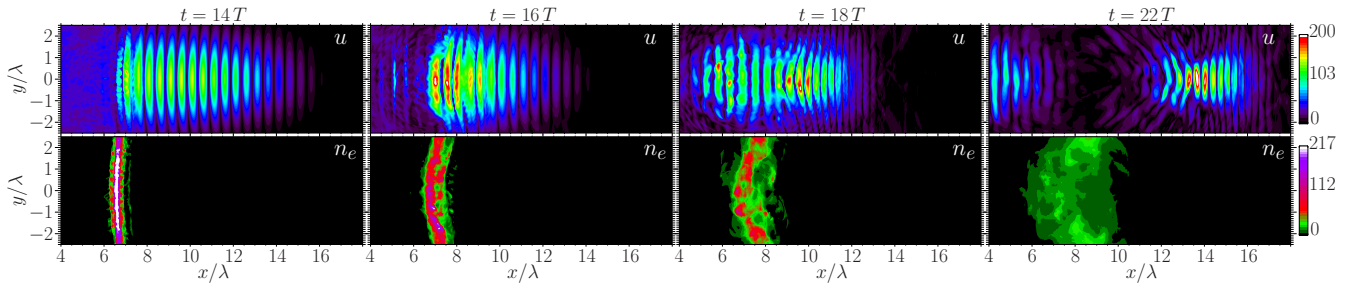


FIG. 2. (color online). Snapshots of $u = \sqrt{(\mathbf{E}^2 + \mathbf{B}^2)}/2$ (first row) and n_e (second row) in normalized units, see the text for details.

denotes the wave number and $k \equiv 2\pi/\lambda$, is reported in Fig. 3(d) (solid, black line) showing that the reflected pulse is chirped and peaked at $\lambda_r \approx 593$ nm. For comparison, the spectra of two Gaussian pulses with the same wavelength and with two (dotted, red line) and three (dashed, blue line) cycles FWHM of the *field* profile are also reported [see Fig. 3(d)].

In order to account for the slowly-rising profile of the source pulse and estimate the wavelength λ_r and peak intensity \hat{I}_r of the reflected pulse, we approximate the \sin^2 -function field profile with a linearly rising profile $b_0 w/N$. Here N is the number of cycles before the source pulse maximum and $b_0 = 3a_s/2\sqrt{2}$ so the source pulse and its linear profile approximation have the same duration and energy before their maximum. Assuming $\mathcal{R}_s \approx 1$, the maximum reflected intensity is achieved at $\min[N, \hat{w}]$ with $\hat{w} = [4Am_p N^2 \zeta_0 / 15\pi Z m_e D_0^+ a_s^2]^{1/3}$. For a slowly-rising profile $\hat{w} \leq N$, thus $\hat{E}_s(\hat{w}) = \zeta_0/5D_0^+$ which *does not* depend on the source pulse parameters. Hence, from Eq. (1) we get $\hat{D}^+(\hat{w}) = 5D_0^+/6$. By inserting our numerical parameters we obtain: $\lambda_r \approx 656$ nm and $\hat{I}_r \approx 1.2 \times 10^{23}$ W/cm² for the linearly rising profile, and $\lambda_r \approx 593$ nm and $\hat{I}_r \approx 1.4 \times 10^{23}$ W/cm² for the more realistic \sin^2 -function profile. While λ_r is in good agreement with the 2D simulation results, \hat{I}_r is underestimated because, by definition, the 1D model does not include focusing effects. Indeed, our simulations show that increasing the ratio σ_d/σ_f by reducing σ_f from 2.6λ to 2.4λ improves the focusing and further enhances \hat{I}_r from 2.3×10^{23} W/cm² to 2.8×10^{23} W/cm². In addition, higher intensities are expected in a fully 3D geometry where, in contrast to 2D simulations, the source pulse is focused also along the z axis. We also mention that increasing $P_{s/d}$ by doubling $\sigma_{s/d}^2$ and σ_f^2 with the other parameters as reported on page 3 enhances \hat{P}_r to 3 PW but reduces the intensity enhancement \hat{I}_r/\hat{I}_s from 2.4 to 1.8 because the pulse focusing decreases.

Finally, we stress that even a few-cycle source pulse can be further shortened and amplified. Indeed, by employing a $\ell_0 = 0.17\lambda$, $\sigma_f = 2.1\lambda$ shaped foil and a driver (source) pulse with 15.5 fs (5.8 fs) duration,

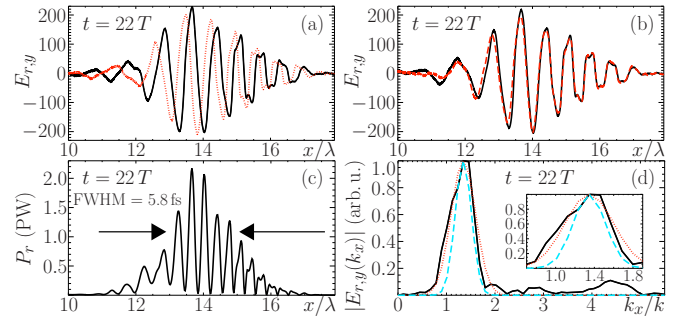


FIG. 3. (color online). Panel (a): $E_{r,y}$ along the central axis for zero (solid, black line) and $\pi/2$ (dotted, red line) CEP of the source pulse. Panel (b): $E_{r,y}$ with RR effects (solid, black line) and with a preplasma on the front surface of the foil (dashed, red line). Panel (c): Power contained in a spot with 1λ radius centered on the axis. Panel (d): $|E_{r,y}(k_x)|$ (solid, black line) and the corresponding quantity for a Gaussian pulse with two (dotted, red line) and three (dashed, blue line) cycles FWHM of the *field* profile. The inset shows a zoom of the main peak region.

$I_d \approx 5.1 \times 10^{22}$ W/cm² ($I_s \approx 5 \times 10^{22}$ W/cm²) intensity and $\sigma_d = 3.1\lambda$ ($\sigma_s = 1\lambda$) radius [corresponding to a driver (source) power $P_d \approx 9.9$ PW ($P_s \approx 1$ PW)], a single 1.5 cycles (2.1 fs duration), 2 J energy, $\hat{P}_r \approx 1.8$ PW and $\hat{I}_r \approx 1.4 \times 10^{23}$ W/cm² reflected pulse is generated ($\hat{I}_s \approx 7 \times 10^{22}$ W/cm²). Moreover, in contrast to the previous case of a relatively long source pulse, a 2.7 fs duration, 1.3 J energy 1 PW peak power and 4.7×10^{22} W/cm² peak intensity transmitted pulse is also generated (see the movies in the Supplemental Material [URL]). Similar parameters for the driver and source pulses are envisaged at the Extreme Light Infrastructure [4, 37].

We acknowledge useful discussions with B. M. Hegelich, N. Kumar, A. Macchi and G. Sarri. We thank A. Macchi for providing his 1D PIC code. Some PIC simulations were performed using the computing resources granted by the Research Center Jülich under the project HRO01.

* matteo.tamburini@mpi-hd.mpg.de

- [1] F. Krausz and M. Ivanov, *Rev. Mod. Phys.* **81**, 163 (2009).
- [2] S. Meuren and A. Di Piazza, *Phys. Rev. Lett.* **107**, 260401 (2011).
- [3] A. I. Titov, H. Takabe, B. Kämpfer, and A. Hosaka, *Phys. Rev. Lett.* **108**, 240406 (2012).
- [4] A. Di Piazza, C. Müller, K. Z. Hatsagortsyan, and C. H. Keitel, *Rev. Mod. Phys.* **84**, 1177 (2012).
- [5] F. Mackenroth and A. Di Piazza, *Phys. Rev. A* **83**, 032106 (2011).
- [6] M. Boca, V. Dinu, and V. Florescu, *Phys. Rev. A* **86**, 013414 (2012).
- [7] A. V. Korzhimanov, A. A. Gonoskov, E. A. Khazanov, and A. M. Sergeev, *Phys. Usp.* **54**, 9 (2011).
- [8] D. Herrmann, L. Veisz, R. Tautz, F. Tavella, K. Schmid, V. Pervak, and F. Krausz, *Opt. Lett.* **34**, 2459 (2009).
- [9] S. Witte and K. Eikema, *IEEE J. Sel. Topics Quantum Electron.* **18**, 296 (2012).
- [10] “Petawatt field synthesizer,” http://www.attoworld.de/Mainpages/Light_and_matter/index.html#42 (2014).
- [11] V. M. Malkin, G. Shvets, and N. J. Fisch, *Phys. Rev. Lett.* **82**, 4448 (1999).
- [12] Z. Toroker, V. M. Malkin, and N. J. Fisch, *Phys. Rev. Lett.* **109**, 085003 (2012).
- [13] L. Lancia, J.-R. Marquès, M. Nakatsutsumi, C. Riconda, S. Weber, S. Hüller, A. Mančić, P. Antici, V. T. Tikhonchuk, A. Héron, P. Audebert, and J. Fuchs, *Phys. Rev. Lett.* **104**, 025001 (2010).
- [14] S. Weber, C. Riconda, L. Lancia, J.-R. Marquès, G. A. Mourou, and J. Fuchs, *Phys. Rev. Lett.* **111**, 055004 (2013).
- [15] J. Faure, Y. Glinec, J. J. Santos, F. Ewald, J.-P. Rousseau, S. Kiselev, A. Pukhov, T. Hosokai, and V. Malka, *Phys. Rev. Lett.* **95**, 205003 (2005).
- [16] J. Schreiber, C. Bellei, S. P. D. Mangles, C. Kamperidis, S. Kneip, S. R. Nagel, C. A. J. Palmer, P. P. Rajeev, M. J. V. Streeter, and Z. Najmudin, *Phys. Rev. Lett.* **105**, 235003 (2010).
- [17] N. L. Wagner, E. A. Gibson, T. Popmintchev, I. P. Christov, M. M. Murnane, and H. C. Kapteyn, *Phys. Rev. Lett.* **93**, 173902 (2004).
- [18] S. A. Skobelev, A. V. Kim, and O. Willi, *Phys. Rev. Lett.* **108**, 123904 (2012).
- [19] V. A. Vshivkov, N. M. Naumova, F. Pegoraro, and S. V. Bulanov, *Phys. Plasmas* **5**, 2727 (1998).
- [20] A. Macchi, S. Veghini, T. V. Liseykina, and F. Pegoraro, *New J. Phys.* **12**, 045013 (2010).
- [21] A. Macchi, S. Veghini, and F. Pegoraro, *Phys. Rev. Lett.* **103**, 085003 (2009).
- [22] P. Mulser and D. Bauer, *High Power Laser-Matter Interaction*, Springer Tracts in Modern Physics, Vol. 238 (Springer, 2010) Chap. 4.2.
- [23] T. Esirkepov, M. Borghesi, S. V. Bulanov, G. Mourou, and T. Tajima, *Phys. Rev. Lett.* **92**, 175003 (2004).
- [24] C. Thaury, F. Quere, J.-P. Geindre, A. Levy, T. Ceccotti, P. Monot, M. Bougeard, F. Reau, P. d’Oliveira, P. Audebert, R. Marjoribanks, and P. Martin, *Nature Phys.* **3**, 424 (2007).
- [25] C. Rödel, M. Heyer, M. Behmke, M. Kübel, O. Jäckel, W. Ziegler, D. Ehrt, M. Kaluza, and G. Paulus, *Appl. Phys. B: Lasers Opt.* **103**, 295 (2011).
- [26] F. Pegoraro and S. V. Bulanov, *Phys. Rev. Lett.* **99**, 065002 (2007).
- [27] S. V. Bulanov, T. Z. Esirkepov, F. Pegoraro, and M. Borghesi, *C. R. Physique* **10**, 216 (2009).
- [28] M. Chen, N. Kumar, A. Pukhov, and T.-P. Yu, *Phys. Plasmas* **18**, 073106 (2011).
- [29] C. A. J. Palmer, J. Schreiber, S. R. Nagel, N. P. Dover, C. Bellei, F. N. Beg, S. Bott, R. J. Clarke, A. E. Dangor, S. M. Hassan, P. Hinz, D. Jung, S. Kneip, S. P. D. Mangles, K. L. Lancaster, A. Rehman, A. P. L. Robinson, C. Spindloe, J. Szerypo, M. Tatarakis, M. Yeung, M. Zepf, and Z. Najmudin, *Phys. Rev. Lett.* **108**, 225002 (2012).
- [30] G. Chériaux, F. Giambruno, A. Fréneaux, F. Leconte, L. P. Ramirez, P. Georges, F. Druon, D. N. Papadopoulos, A. Pellegrina, C. Le Blanc, I. Doyen, L. Legat, J. M. Boudenne, G. Mennerat, P. Audebert, G. Mourou, F. Mathieu, and J. P. Chambaret, *AIP Conf. Proc.* **1462**, 78 (2012).
- [31] A. V. Krasheninnikov and F. Banhart, *Nature Mater.* **6**, 723 (2007).
- [32] W. van Dorp, C. Hagen, P. Crozier, B. van Someren, and P. Kruit, *Microelectron. Eng.* **83**, 1468 (2006).
- [33] M. Chen, A. Pukhov, T. P. Yu, and Z. M. Sheng, *Phys. Rev. Lett.* **103**, 024801 (2009).
- [34] M. Chen, T.-P. Yu, A. Pukhov, and Z.-M. Sheng, *New J. Phys.* **12**, 045004 (2010).
- [35] M. Tamburini, F. Pegoraro, A. Di Piazza, C. H. Keitel, and A. Macchi, *New J. Phys.* **12**, 123005 (2010).
- [36] M. Tamburini, T. V. Liseykina, F. Pegoraro, and A. Macchi, *Phys. Rev. E* **85**, 016407 (2012).
- [37] “Extreme light infrastructure,” <http://www.eli-laser.eu/> (2014).